THE JOURNAL OF PHYSICAL CHEMISTRY Letters

Letter

pubs.acs.org/JPCL

Unraveling the Mechanism of Photoinduced Charge Transfer in Carotenoid–Porphyrin–C_{60} Molecular Triad

Arun K. Manna,[†] D. Balamurugan,[‡,∥] Margaret S. Cheung,*[,‡,§] and Barry D. Dunietz*[,†]

[†]Department of Chemistry, Kent State University, 1787 Summit Street, Kent, Ohio 44242, United States

[‡]Department of Physics, University of Houston, 617 Science & Research Building 1, Houston, Texas 77204, United States

[§]Center for Theoretical Biological Physics, Rice University, 6500 Main Street, Houston, Texas 77030, United States

[∥]Computation Institute, University of Chicago, 5735 South Ellis Avenue, Chicago, Illinois 60637, United States

Supporting Information

ABSTRACT: Photoinduced charge transfer (CT) plays a central role in biologically significant systems and in applications that harvest solar energy. We investigate the relationship of CT kinetics and conformation in a molecular triad. The triad, consisting of carotenoid, porphyrin, and fullerene is structurally flexible and able to acquire significantly varied conformations under ambient conditions. With an integrated approach of quantum calculations and molecular dynamics simulations, we compute the rate of CT at two distinctive conformations. The linearly extended conformation, in which the donor (carotenoid) and the acceptor (fullerene) are separated by nearly 50 Å, enables charge separation through a sequential CT process. A representative bent conformation that is entropically dominant, however, attenuates the CT, although the donor and the acceptor are spatially closer. Our computed rate of CT at the linear conformation is in good agreement with measured values. Our work provides unique fundamental understanding of the photoinduced CT process in the molecular triad.

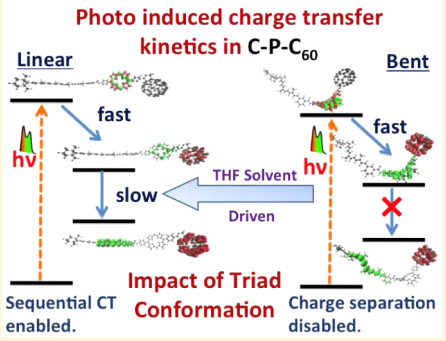

Almost all chemical reactions involve a degree of CT designating molecular regions as the donor and the acceptor of the charge. The redistribution of electronic charges depends on the molecular structure and the effect of the surrounding environment on the electronic density. Solar-induced CT processes in donor–acceptor molecular systems lie at the foundation of emerging technologies based on organic semiconductors and define the functionality of biologically significant molecular systems;[1−5] however, these complex molecular systems are known to yield a broad ensemble of conformations under ambient conditions, thus inevitably affecting the CT process. As a result, a molecular level understanding of the photoinduced CT processes in the presence of structural variations is critical for advancing related technologies.[6−11]

A widely studied CT system is a bioinspired molecular triad consisting of covalently linked carotenoid polyene (C), diaryl porphyrin (P), and fullerene (C_{60}) first synthesized in 1997.[12,13] (See the illustration in Figure 1.) The molecular triad absorbs a UV–visible light and produces a charge-separated state (CT2) where an electron is transferred from C to C_{60} (C^{+}–P–C_{60}^{-}), thus producing a large dipole moment of ∼150 D.[14,15] The large dipole and the long lifetime on the order of nanoseconds of the accessible charge-separated state elevate the promise of using the triad for applications that harvest solar energy.[12,13,15,16]

The molecular consistency of the triad complicates its structure–function relationships, affecting the generation of

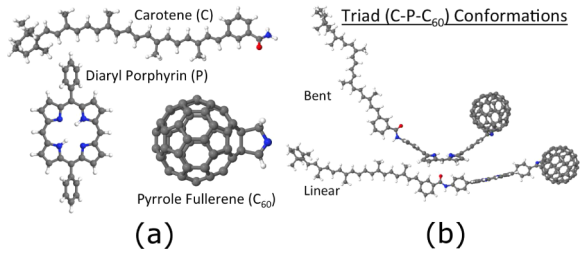

Figure 1. (a) Molecular structure of three chemical moieties of the triad: carotene (C), diaryl-porphyrin (P) and pyrrole-fullerene (C_{60}) (b). Two key conformations of triad (C–P–C_{60}): Linearly and bent conformations.

charge separation, where a complex sequential process is indicated.[13,16] In these studies the charge-separated state (CT2 state) follows the porphyrin excitation on the tens to hundreds of picoseconds time scale.[13,16] Quantum dynamics (QD) simulations propagating LDA-based DFT descriptions[10,17] on the subpicosecond time scale following the excitation of the porphyrin system find a semiseparated CT state (CT1), which involves the bridging P as the donor (C–P^{+}–C_{60}^{-}), being accessed. More recently QD simulations on the larger time scale based on an semiempirical approach confirm the

Received: January 14, 2015
Accepted: March 17, 2015
Published: March 17, 2015

DOI: 10.1021/acs.jpclett.5b00074
J. Phys. Chem. Lett. 2015, 6, 1231−1237

subsequent generation of the fully charge-separated CT2 state on the hundreds of picoseconds time scale from the fast generated CT1 state.[18] Several computational studies confirm the importance of intramolecular modes in affecting the kinetics. Early DFT and time-dependent density function theory (TDDFT) investigated the CT states in the linearly extended conformation and a molecular J-shaped conformation.[17,19,20] Cheung et al. further found a wide structural distribution of the triad in explicit water[21] and tetrahydrofuran (THF)[22] using molecular dynamics simulations. Thermal fluctuations facilitate the transition between a linearly extended configuration, which is the most energetically stable one, to a bent configuration that is, however, the dominant one at room temperature due to entropy. More recently the triad structural flexibility to affect dipole and therefore the expected CT dynamics involved in charge separation has been analyzed using LDA-based DFT,[23] therefore confirming the role of nuclei modes on charge separation, as indicated by the QD simulation of the CT1 state.[18]

Here we address the following key question: How does the photoexcited molecular triad C−P−C_{60} in solvent achieve its fully charge-separated state given its structural flexibility? Importantly, we identify the linear and bent structures as two key conformations of the triad (see their illustration in Figure 1b) that differ substantially in their photoinduced kinetics generating the charge-separated state. Furthermore, according to our findings, while structural flexibility may strongly affect the kinetics, the key modes in the CT mechanism are indicated to be intermolecular solvent-based.

We employ a comprehensive scheme that is designed to address the underlying challenges due to the difficulty in modeling CT states and the conformational flexibility. (Further details of the state-of-the-art modeling tools to address these complexities are provided in the Supporting Information (SI) Section I and are outlined next.)

The first challenge emerges from the tendency of standard DFT to underestimate the energies of CT states in the gas phase. This caveat is exacerbated by the need to address the polar environment that strongly affects the CT states. Previous electronic structure studies of the triad low-lying CT states were based on such standard functionals.[10,17,19,20,23] To overcome these difficulties, Dunietz's group recently implemented an approach based on TDDFT employing a range-separated hybrid (RSH) functional where the solvent effects on the CT states are accounted for using charge-constraint DFT (CDFT)[24] calculations within a polarized continuum model (PCM).[25,26] This combined scheme was shown to produce good agreement of calculated solvated CT state energies with relevant measurements[27−29] and in the parametrization of rates of photoinduced CT processes.[30−33]

The second challenge arises at the molecular level due to the accessible myriad of triad conformations. Large variations in the experimentally measured dipole moment of the excited state (110−160 D)[15,34] confirm the formation of a conformational ensemble of the triad in a solution of reverse micelles. This conformational flexibility dictates the relative orientation of the moieties, which may strongly affect CT processes. Entropic effects due to the solvents were found to play an important role in charge separation.[34] A recent study showed that the correlated motion of electrons and nuclei plays an important role in the CT process of the C−P−C_{60} triad;[10] however, there still remains a gap in understanding how the excited-state properties are affected by the indicated conformational flexibility.

We developed a computationally comprehensive approach to acquiring a molecular level insight into the relationship between the molecular conformation and the CT processes in the molecular triad. A schematic illustration of the relevant potential energy surfaces in a photoinduced CT process is shown in Figure 2a. As illustrated, a polar environment (e.g., a

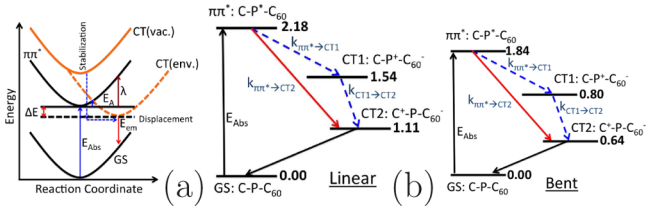

Figure 2. (a) Environment-affected CT potential energy surfaces: Increased ΔQ may (i) increase geometric displacement (λ) or (ii) increase the force for transfer (ΔE) by energetic stabilization. (b) Energies of the solvated electronic excited states for both linear and bent triad conformations: Two possible pathways (solid and dotted lines) leading to the final fully charge-separated (CT2) state are found. Energies are in eV.

polar THF solvent as used in the experiment) stabilizes the CT state relative to the excitonic states. This stabilization manifests in two key energetic parameters: (a) The free-energy drive (ΔE) between the excitonic state and the photoinduced CT product and (b) the reorganization energy (λ) that reflects the extent of structural relaxation. These two energetic parameters are affected by the amount of the transferred charge and the alignment of the CT state energy relative to that of the excitonic state. Recently we have investigated the relationship of charge separation and solvent polarity to affect these key energetic parameters and therefore to determine the CT rate.[32]

The rate of the photoinduced CT (k_M) in the normal regime (and the non-far-inverted regime) depends on the ΔE and λ energies as prescribed by the seminal semiclassical Marcus expression[35−37]

$$k_M = \frac{|V|^2}{\hbar}\sqrt{\frac{\pi}{k_B T\lambda}}\exp\left[-\frac{E_A}{k_B T}\right] \quad (1)$$

$E_A = (\Delta E+\lambda)^2/(4\lambda)$ is the activation energy for crossing to the product state, and V denotes the electronic coupling between the two electronic states.

The linear and bent models that represent two key triad conformations differ substantially in the kinetics, leading to the charge-separated state. The linearly extended conformation is energetically favorable and consistent with the DFT-optimized conformation. The bent conformation represents an entropically favored population found in molecular dynamics simulations with explicit THF solvent.[22] (Several key structural differences between the two conformations are listed in SI Section II.) Shifts in their population under ambient conditions depend on the triad CT state and the solvent. For example, photoexcitations favor the linear conformation in THF.[22] We calculate the solvation energies of the two main conformations using MD simulations (further description of the setup is provided in the appendix and SI). We investigate the effect of varied conformation on the kinetics of the photoinduced CT and address the role of energetic versus entropic conforma-

DOI: 10.1021/acs.jpclett.5b00074
J. Phys. Chem. Lett. 2015, 6, 1231−1237

Table 1. Excitation Energies for Absorbing (E_{Abs}) and Charge-Transfer (E_{CT}) States in the Gas Phase[a]

system	functional	E_{Abs}(gas)	E_{CT}(gas)	ΔQ (e)	E_s	E_{CT}(sol)	$E_{CT'}$(sol)
linear-triad	BNL	2.18 (0.125), 2.41 (1.933) [P]	2.50 (0.001) [CT1]	0.72	0.88	1.62	1.54
	BNL	2.19 (0.004) [C_{60}] and 2.44 (4.152) [C]	2.54 (0.000) [CT2]	0.99	1.26	1.28	1.11
	B3LYP	2.19 (0.956) [P] and 1.48 (0.000) [C_{60}]	1.25 (0.001) [CT1]	0.99			
	B3LYP	2.23 (3.907) [C]	0.73 (0.000) [CT2]	0.99			
bent-triad	BNL	1.84 (0.563), 1.93 (0.186) [P]	1.77 (0.130) [CT1]	0.84	0.89	0.88	0.80
	BNL	1.65 (0.004) [C_{60}] and 2.63 (3.671) [C]	2.36 (0.000) [CT2]	0.99	1.55	0.81	0.64
	B3LYP	1.83 (0.371) [P], 1.91 (0.284) [P]	0.65 (0.007) [CT1]	0.99			
	B3LYP	1.49 (0.003) [C_{60}] and 2.39 (1.27) [C]	0.68 (0.000) [CT2]	0.99			

[a]Values within parentheses indicate oscillator strength of the excitation. The amount of charge transferred (ΔQ) and THF solvent-corrected CT energies at the solvent-affected ground-state geometry (E_{CT}(sol)) and at the corrected charge-separated geometry ($E_{CT'}$(sol)) are tabulated. Solvation energies (E_s) are also listed. The experimentally measured low-lying excited-state energies are 2.4 (C), 1.9, and 2.1 (Q) and 1.6 (CT1) and 1.0 (CT2).[13] All energies are given in electronvolts.

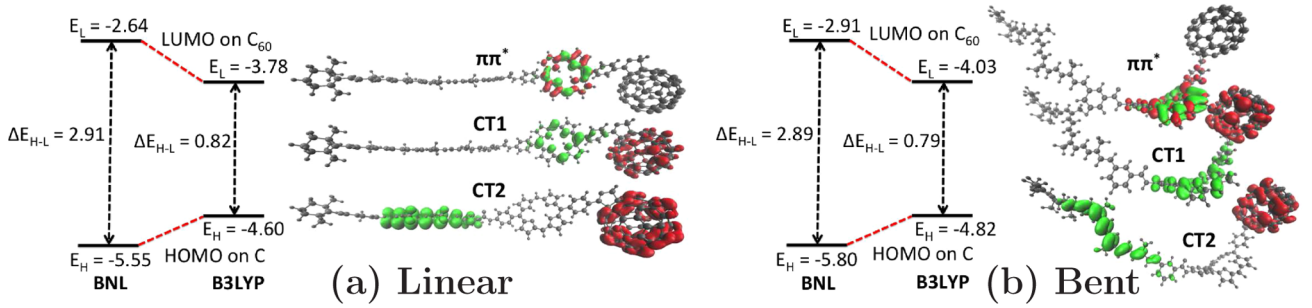

Figure 3. Linear (a) and bent (b) HOMO and LUMO energies (BNL and B3LYP functionals). All energies are reported in eV. The nature of the different electronic excitations ($\pi-\pi*$ and CT) is illustrated by plotting the corresponding detachment/attachment densities using the BNL functional.

tional preference by studying both the sequential and concerted CT mechanisms at both conformations.

The excited-state energies vary between the two conformations, as detailed in Table 1 and illustrated in Figure 2b. The relevant MOs to the low-lying excited states are plotted in SI Figure S1. The corresponding orbital energy gaps are listed for the low-lying CT states in SI Table S1, where the fundamental gaps are illustrated in Figure 3. The physical significance of the BNL orbitals is established, where the energies of the FMOs correspond properly to the IP (HOMO) and EA (LUMO).[29,38−40] We emphasize that the triad spectra correspond to combining the spectral lines of the separated moieties,[17,19] confirming a weak coupling between the moieties. We also provide for completeness the values for the monomers in SI Table S2. Indeed the FMOs as illustrated are well-separated and localized on the different chemical moieties of the triad.

For the linear conformation we identified three low-energy bright (with considerable oscillator strength) states with 2.18, 2.41, and 2.44 eV excitation energies corresponding to the two Q-band electronic states of porphyrin and the carotenoid $\pi-\pi^*$ state, respectively. These states were calculated using TDDFT with the RSH BNL functional. The calculated electronic spectra are in good agreement with experimental measurements featuring the characteristic porphyrin Q band in the 1.9 to 2.1 eV range and the main peak of carotene at 2.4 eV.[13] The bent conformation with the distorted P results in an increased energetic difference within the lowest band of excited states (Q band), which results in a lower lowest excited-state energy than that found for the linear conformation (Q states of 1.84 and 1.94 eV). The calculated absorbing state energy related to the carotenoid is 2.63 eV, which is also a small change from the value in the linear conformation. This trend observed for the bent spectra is in agreement with a recent exhaustive investigation of conformational effects on the triad CT states energies.[23] Results confirming these observations on several bent conformations are presented in SI Section III.

There are two CT states that are present in either conformation, where CT1 ($C-P^+-C_{60}^-$ with an electron on C_{60} and a hole on porphyrin) is of a shorter range of transfer and CT2 ($C^+-P-C_{60}^-$ with the hole on C) is of the longer distance separation. The attachment and detachment electronic densities related to the low-lying excited states at both conformations are illustrated in Figure 3. The CT1 involves electron promotion from HOMO−1 to LUMO, and CT2 involves electron promotion from HOMO to LUMO. (The related FMOs are illustrated in SI Figure S1.)

Both CT1 and CT2 states are present in either conformation. The CT states are almost degenerate in the linear conformation with 2.50 and 2.54 eV excitation energies and with lower energies in the bent conformation with 1.77 and 2.36 eV. The main impact of the structural deformation in the bent conformation is to decrease the excitation energies for the CT1 state quite substantially, where it affects to a lesser degree the P excitonic states and the CT2 state. According to the Mülliken population analysis, at the linear conformation 0.72 (0.99) electrons are transferred in the CT1 (CT2) states. At the bent structure, 0.84 (0.99) electrons are transferred.

The energies of the solvated CT states (1.54 and 1.11 eV for CT1 and CT2) are also in good agreement with the measured cyclovoltammetry energies of 1.58 and 1.03 eV.[13] The CT energies are illustrated in Figure 2 and listed along with the solvation energies in Table 1 with further discussion in SI Section IV. In SI Figure S3 we provide a snapshot of a

DOI: 10.1021/acs.jpclett.5b00074
J. Phys. Chem. Lett. 2015, 6, 1231−1237

Table 2. Charge Separation (ΔQ), FCD Electronic Coupling (V), solvation Energy (E_s), Solute (λ_i), Solvent (λ_e), and Total ($\lambda = \lambda_i + \lambda_e$) Reorganization Energies, Driving force (ΔE), Activation Energy (E_A), and Marcus CT Rates (k_M) Calculated at Room Temperature for the Two Triad Conformations[a]

triad	ΔQ (e)	CT reaction	V (eV)	E_s (eV)	λ_i (eV)	λ_e (eV)	λ (eV)	ΔE (eV)	E_A (eV)	k_M (s^{-1})
linear	0.72 (CT1)	($\pi\pi^*$ → CT1)	9.0×10^{-3}	0.88	0.08	0.74	0.82	−0.64	0.009	1.0×10^{12}
	0.99 (CT2)	($\pi\pi^*$ → CT2)	2.0×10^{-4}	1.26	0.17	1.22	1.39	−1.07	0.019	2.7×10^{8}
		(CT1 → CT2)	1.0×10^{-3}	0.19	0.08	1.08	1.16	−0.60	0.067	1.1×10^{9}
bent	0.84 (CT1)	($\pi\pi^*$ → CT1)	2.4×10^{-2}	0.89	0.08	0.50	0.58	−1.04	0.092	3.4×10^{11}
	0.99 (CT2)	($\pi\pi^*$ → CT2)	4.5×10^{-5}	1.55	0.17	1.38	1.55	−1.19	0.021	1.2×10^{7}
		(CT1 → CT2)	8.6×10^{-5}	0.70	0.08	1.48	1.56	−0.33	0.243	6.6×10^{3}

[a]The experimental measured rates[15] are as follows: $k(\pi\pi^* \rightarrow \text{CT1}) = 3.3 \times 10^{11}\ s^{-1}$ and $k(\text{CT1} \rightarrow \text{CT2}) = 1.5 \times 10^{10}\ s^{-1}$.

trajectory used to obtain the averaged solvation energy involving the interaction of the triad atoms with the explicit solvent molecules for each conformation. The energetic ordering of the THF solvated states for both triad conformations is as follows: $E_{\pi-\pi^*} > E_{CT1}(sol) > E_{CT2}(sol)$ and is as expected because the solvation energy increases with dipole strength, where the CT2 dipole is the largest. The same trend in the ordering of the excited states is observed for other optimized solvated geometries, with, however, some substantial differences in the CT energies between the conformations, where the bent CT1 energy is 0.8 eV lower.

The calculated electronic coupling strengths between either CT1 or CT2 states to an excitonic state suggest (see Table 2) two possible mechanisms for the photoinduced charge transfer: In one mechanism, the charge separation follows a series of CT steps, where CT2, which is the final charge-separated state, is produced following coupling to CT1. The second mechanism involves a single concerted step where the final CT2 state is directly coupled to the absorbing state of a localized $\pi-\pi^*$ excitation on the porphyrin chromophore.

The electronic coupling to the CT2 states of the excitonic $\pi-\pi^*$ state is substantially lower in the bent conformation than in the linear one, whereas the overall coupling to the CT1 states increases (values listed in Table 2). The V coupling at the linear and bent conformations for the $\pi-\pi^* \leftrightarrow$ CT1 process is 9.2×10^{-3} and 2.4×10^{-2} eV, respectively. The $V(\pi-\pi^* \leftrightarrow \text{CT2})$ are 2.0×10^{-4} and 4.5×10^{-5} eV (linear and bent, respectively), and for CT1 ↔ CT2 these are 1.6×10^{-3} and 8.6×10^{-5} eV (linear and bent). This trend of a lower coupling strength for the bent conformation is mainly due to the structural distortion of the carotene chain. (A detailed study of the structural features that strongly affect the coupling strength is provided in the SI Section V). We hypothesize that the triad spatial conformation strongly affects the process of charge separation of a molecular triad. The importance of conformational changes is confirmed later by comparing the computed rate constants of CT processes of either mechanism.

The photoinduced CT kinetics is modeled following the semiclassical picture of the Marcus theory.[37] Only in the far-inverted regime, where $\Delta E \gg \lambda$, are quantum corrections necessary in calculating the rate constants.[30] In this study, with one exception described later, the rates are well-described by the semiclassical expression of eq 1 and therefore parametrized by the driving force (ΔE) and the reorganization (λ) energies. These energetic parameters and the resulting charge-transfer rate constants are shown in Table 2 for both the linearly extended and the bent conformations along with the experimentally measured rate constants.[15]

The reorganization and driving force energies increase with the amount of the charge transferred; therefore, both terms are larger for CT2 than for CT1. Indeed this trend is as expected, where the larger dipole in CT2 is further stabilized by polar solvent over the solvent stabilization afforded for CT1. The role of intramolecular polarization in charge separation in the triad was analyzed using QD simulations with an extended Hückel model.[10]

For all considered CT processes the driving force is larger in the bent conformation than in the linear one, except for the CT1→ CT2 process. This trend results from the substantially smaller CT excitation energies in the bent case. The calculated internal reorganization energies (λ_i) at the linear conformation are small (<0.2 eV), where we are assuming the same values for the bent conformation. The λ_i is confirmed to be much smaller than the solvent reorganization energy (λ_e). Substantial differences between the two conformations are found due to the solvent modes. The λ_e energies that are obtained using classical MD simulations are of 0.8 and 0.5 eV for the CT1 process and of 1.4 and 1.2 eV for the CT2 process at the linear and bent conformations, respectively. For CT2 the λ_e energies are larger because of the increased charge separation.

For the linear conformation the rate constant for the $\pi-\pi^*$ → CT1 reaction of $1.0 \times 10^{12}\ s^{-1}$ is three to four orders of magnitude larger than the rates for the $\pi-\pi^*$ → CT2 and CT1→ CT2 reactions. The rate for the CT1→ CT2 reaction of $1.1 \times 10^{9}\ s^{-1}$ is one order of magnitude larger than the $\pi-\pi^*$ → CT2 value. This suggests a two-step sequential CT process ($\pi-\pi^*$ → CT1→ CT2) for the linear conformation. The calculated CT rates of the sequential mechanism are in relatively good agreement with the experimental measured rates,[13,15] where CT1 is reached at the subpicosecond time scale, followed by transfer to CT2 on a two to three times slower time scale. (See the values in Table 2.)

In contrast, the CT processes in the bent configuration are slower than those of the linear conformation. Although the charge transfer to CT1 seems to dominate, the following CT1→ CT2 step is substantially slower at the order of milliseconds. We point out that the $\pi-\pi^*$ → CT1 is in the inverted regime (the only process in our study); therefore, the calculated rate may underestimate the actual value, although we find that it is not in the far-inverted regime that would require quantum-mechanical corrections.[5,30,33] This remains only of a minor concern because the following step is very slow (and not in the inverted regime), indicating that the sequential mechanism is practically turned off in the bent conformation. Therefore, the CT1 in the bent conformation functions as a charge trap, further hindering the generation of charge separation in CT2. Consequently, the concerted mechanism may become the dominant mechanism for charge separation for the bent conformation, although the calculated rate for the concerted mechanism in the bent conformation remains smaller

DOI: 10.1021/acs.jpclett.5b00074
J. Phys. Chem. Lett. 2015, 6, 1231−1237

than that of the linear one. We therefore conclude that overall the photoinduced-production of the charge-separated state is disabled in the bent conformation. We confirmed that this trend exists for several other bent conformations, which were also taken from our previous molecular dynamics simulations.[22] (See SI Tables S3 and S4 demonstrating the minor effect on the spectra and coupling strength due to a varied bent conformation.)

Triad CT Kinetics Modeling Discussion. First we address our finding that the intermolecular solvent-mode-based reorganization energy is dominant over the intramolecular triad-mode-based reorganization energy. While our simulated rates and calculated spectra are in agreement with experimental measurements, we point out that this finding is in contrast with previous QD simulations that find intramolecular vibrational coupling effects to play a dominant role in the CT mechanism.[10] We therefore suggest that the role of vibrational coupling in the CT should be further investigated. Our electronic spectra modeling employs RSH-based DFT that is corrected for the solvation, where for the QD simulation LDA-based DFT was employed. Using the LDA in TDDFT is known to underestimate CT state energies (and therefore overestimate the CT processes).

Importantly, the modeling of the kinetics rather than pursuing the complex full dynamics of the system enabled us to calculate high-quality potential energy surfaces and to generate a novel perspective on the CT mechanism; however, there are several limitations and approximations in our approach that should be carefully considered to fully grasp the CT mechanism in this system. In the present work we assume that the internal reorganization energy for the bent conformations is the same as that calculated for the linear conformation. This assumption should be lifted before a final conclusion on the relative role of inter- to intra-vibrational coupling effects can be drawn. This requires a more comprehensive MD sampling scheme combined with QM/MD simulations, where the triad is used to define the QM region and is treated with the same electronic structure protocol as provided in this study. The more complete analysis of intramolecular vibronic coupling will also require addressing possible nonequilibrated (NE) population of the normal modes. NE vibronic state populations are expected to affect especially the second CT step (CT1 to CT2). NE extensions can be used to calculate the intramolecular reorganization energy of the bent conformation because the linear conformation is the most stable one. Addressing the different NE effects requires in addition to the electronic structure and MD developments the implementation of more complete Fermi golden rule relations. Another NE aspect that can be addressed by more elaborate QM/MD simulations includes the conformational redistribution of the excitonic bands that have been ignored in this study. Efforts to address these limitations and approximations are pursued by our groups.

In summary, using combined approach we studied the relationships of structure−property that affect the photo-induced charge-transfer kinetics in a molecular triad C−P−C_{60}. We analyzed the properties of two representative conformations (linearly extended and bent) to understand the mechanism behind several experimental observations. For the linear conformation, the CT kinetics is dominated by a two-step sequential mechanism, where the shorter range CT state (CT1), which is accessed on the subpicosecond time scale, is followed by the longer range CT state (CT2) on the several tenths of a picosecond time scale, in agreement with previous experimental and computational studies.[10,13,16,18] The CT mechanisms indicated from the modeling of the kinetics rather than the full dynamical perspective suggest that the transfer depends on solvent-based intermolecular modes. We stress that the kinetics modeling employs RSH functional that implements modern DFT to afford reliable treatment of CT states energies.

While the CT mechanism is found to be driven by intermolecular solvent-based modes, we find that the intramolecular triad conformation may greatly affect the CT kinetics. For the bent conformation the charge transfer is attenuated due to a significantly reduced rate for the transfer process between the shorter and longer range CT states (CT1 ↔ CT2). Our findings, therefore, encourage developing strategies to populate linear conformations over the bent ones for achieving efficient charge separation. This can be implemented, for example, by decreasing the solvent dielectrics,[22] although reduced polarizing environment may also change the associated energetic stabilization and therefore the rate kinetics. Nonetheless, such molecular level insight into charge-transfer mechanisms in malleable molecular triads bears the potential for a far-reaching impact on efforts to design materials for improved optoelectronic applications. Indeed, in a recent collaborative effort we investigated the interfacial structural effect in OPV devices that were fabricated by reversing the order of depositing the organic donor and acceptor thin layers. These devices demonstrated optical and transfer activities that depend strongly on the fabrication scheme.[41]

■ APPENDIX

In this section we provide further details of the computational methods:

Quantum Calculations. The electronic structure optimizations were performed using DFT combined with polarizable continuum model employing B3LYP[42−45] hybrid functional with split-valence (SV) basis set for all atoms. We employed modern TDDFT using an RSH functional to reliably describe the energies of the CT states. We used the BNL functional, developed by Baer, Neuhauser, and Livshits[38−40] at the SV basis set level. In calculating the BNL tuning parameter (γ) we adopted the J2 error minimization scheme.[46] The electronic couplings from TDDFT were calculated by the fragment charge difference (FCD) method[47] with TD-BNL-based excited-state densities. The lowest CT state geometry was obtained using CDFT, where the electrostatic environment presented by the solvent was modeled with PCM.[25,26] The PCM was implemented using switching gaussians for spatial discretization that was shown to achieve robust solvated electronic densities,[48−50] where the charge constraints were determined by the TDDFT calculations of the relevant excited state.

Molecular Dynamics Simulations. Molecular dynamics simulations of the triad molecule in THF solvent were performed to obtain the solvation energies for the charge-transfer reactions by following a two-state protocol.[51] We extracted the free energy and reorganization energy for the charge-transfer reactions in the triad molecule by following the linear response approximation.[51−53] The free-energy difference (ΔG) and external (solvent) reorganization energy (λ_e)[51] for the computation of the charge-transfer reaction (a → b) are given by

DOI: 10.1021/acs.jpclett.5b00074
J. Phys. Chem. Lett. 2015, 6, 1231−1237

$$\Delta G = \frac{1}{2}[\langle V_b - V_a\rangle_a + \langle V_b - V_a\rangle_b] \quad (2)$$

$$\lambda_e = \frac{1}{2}[\langle V_b - V_a\rangle_a - \langle V_b - V_a\rangle_b] \quad (3)$$

where a and b represents the reactant and the product states. V_a and V_b are the potential energies of the reactant and the product states. The averages $\langle ...\rangle_a$ and $\langle ...\rangle_b$ were evaluated over the simulated trajectories of reactant state a and product state b at their individual equilibrium conditions, respectively. In the average $\langle V_b - V_a\rangle_a$, the energy gap was calculated at state a, where V_a was evaluated at equilibrium and V_b was evaluated out of equilibrium. Further details of the MD sampling techniques are given in SI Section VI and the references.

■ ASSOCIATED CONTENT

Supporting Information

Modeling challenges, structural differences between the linear and bent triad conformations, electronic spectra and coupling strengths, solvation energies and frontier molecular orbital (FMO) energies, and plots for the linear and bent triad conformations. We also provide the monomer (carotene, diaryl-porphyrin, and pyrrole-C_{60}) excitations energies and the *XYZ* Cartesian coordinates of the different conformations. This material is available free of charge via the Internet at http://pubs.acs.org.

■ AUTHOR INFORMATION

Corresponding Authors

*E-mail: mscheung@central.uh.edu.

*E-mail: bdunietz@kent.edu.

Notes

The authors declare no competing financial interest.

■ ACKNOWLEDGMENTS

M.S.C. and B.D.D. acknowledge awards from the Department of Energy (DOE) - Basic Energy Sciences through the Chemical Sciences Geosciences and Biosciences Division: award numbers DE-SC0004924 and DE-FG02-10ER16174 (B.D.D.) and award number DE-FG02-10ER16175 (M.S.C.). B.D.D. thanks the Ohio supercomputer for making a computing resource available and Kent State University for making the College of Arts and Sciences computing resource available. D.B. acknowledges the computing resources of XSEDE (TG-DMR130015). This research used resources of the National Energy Research Scientific Computing Center, which is supported by the Office of Science of the U.S. Department of Energy under contract no. DE-AC02-05CH11231.

■ REFERENCES

(1) Barbara, P. F.; Meyer, T. J.; Ratner, M. A. Contemporary Issues in Electron Transfer Research. *J. Phys. Chem.* **1996**, *100*, 13148−13168.

(2) Chandler, D. Electron Transfer in Water and Other Polar Environments, How It Happens. In *Classical and Quantum Dynamics in Condensed Phased Simulations: Proceedings of the International School of Physics "Computer Simulation of Rare Events and Dynamics of Classical and Quantum Condensed-Phased Systems"*; Berne, B. J., Cicootti, G., Coker, D. F., Eds.; World Scientific: River Edge, NJ, 1998; Chapter 2, pp 25−50.

(3) Weiss, U. *Quantum Dissipative Systems*; World Scientific: London, 1993.

(4) May, V., Kühn, O. *Charge and Energy Transfer Dynamics in Molecular Systems*; Wiley-VCH: Berlin, 2000.

(5) Nitzan, A. *Chemical Dynamics in Condensed Phases*; Oxford University Press: New York, 2006.

(6) Dou, L.; You, J.; Yang, J.; Chen, C.-C.; He, Y.; Murase, S.; Moriarty, T.; Emery, K.; Li, G.; Yang, Y. Tandem Polymer Solar Cells featuring a Spectrally Matched Low-Bandgap Polymer. *Nat. Photon* **2012**, *6*, 180−185.

(7) Troisi, A.; Orlandi, G. Charge-Transport Regime of Crystalline Organic Semiconductors: Diffusion Limited by Thermal Off-Diagonal Electronic Disorder. *Phys. Rev. Lett.* **2006**, *96*, 086601.

(8) Thompson, A.; Ahn, T.-S.; Justin, K. R.; Thayumanavan, T. S.; Martínez, T. J.; Bardeen, C. J. Using Meta Conjugation To Enhance Charge Separation versus Charge Recombination in Phenylacetylene Donor-Bridge-Acceptor Complexes. *J. Am. Chem. Soc.* **2005**, *127*, 16348−16349.

(9) Jailaubekov, A. E.; et al. Hot Charge-Transfer Excitons set the Time limit for Charge Separation at Donor/Acceptor interfaces in Organic Photovoltaics. *Nat. Mater.* **2013**, *12*, 66−73.

(10) Rozzi, C. A.; et al. Quantum Coherence Controls the Charge Separation in a Prototypical Artificial Light-harvesting System. *Nat. Commun.* **2013**, *4*, 1−7.

(11) Falke, S. M.; et al. Coherent Ultrafast Charge Separation in an Organic Photovoltaic Blend. *Science* **2014**, *344*, 1001−1005.

(12) Liddell, P. A.; Kuciauskas, D.; Sumida, J. P.; Nash, B.; Nguyen, D.; Moore, A. L.; Moore, T. A.; Gust, D. Photoinduced Charge Separation and Charge Recombination to a Triplet State in Carotene-Porphyrin-Fullerene Triad. *J. Am. Chem. Soc.* **1997**, *119*, 1400−1405.

(13) Kodis, G.; Liddell, P. A.; Moore, A. L.; Moore, T. A.; Gust, D. Synthesis and Photochemistry of a Carotene-porphyrin-fullerene model Photosynthetic Reaction Center. *J. Phys. Org. Chem.* **2004**, *17*, 724−734.

(14) Kuciauskas, D.; Liddell, P. A.; Lin, S.; Stone, S. G.; Moore, A. L.; Moore, T. A.; Gust, D. Photoinduced Electron Transfer in Carotenoporphyrin-Fullerene Triads: Temperature and Solvent Effects. *J. Phys. Chem. B* **2000**, *104*, 4307−4321.

(15) Smirnov, S. N.; Liddell, P. A.; Vlassiouk, I. V.; Teslja, A.; Kuciauskas, D.; Braun, C. L.; Moore, T.; Gust, D. Characterization of the Giant Transient Dipole Generated by Photoinduced Electron Transfer in a Carotene-Porphyrin-Fullerene Molecular Triad. *J. Phys. Chem. A* **2003**, *107*, 7567−7573.

(16) Gust, D.; Moore, T. A.; Moore, A. L. Mimicking Photosynthetic Solar Energy Transduction. *Acc. Chem. Res.* **2001**, *34*, 40−48.

(17) Spallanzani, N.; Rozzi, C. A.; Varsano, D.; Baruah, T.; Pederson, M. R.; Manghi, F.; Rubio, A. Photoexcitation of a Light-Harvesting Supramolecular Triad: A Time-Dependent DFT Study. *J. Phys. Chem. B* **2009**, *113*, 5345−5349.

(18) Rego, L. G. C.; Hames, B. C.; Mazon, K. T.; Joswig, J.-O. Intramolecular Polarization Induces Electron-Hole Charge Separation in Light-Harvesting Molecular Triads. *J. Phys. Chem. C* **2014**, *118*, 126−134.

(19) Baruah, T.; Pederson, M. R. DFT Calculations on Charge-Transfer States of a Carotenoid-Porphyrin-C_{60} Molecular Triad. *J. Chem. Phys.* **2006**, *125*, 164706−164710.

(20) Baruah, T.; Pederson, M. R. DFT Calculations on Charge-Transfer States of a Carotenoid-Porphyrin-C_{60} Molecular Triad. *J. Chem. Theor. Comput.* **2009**, *5*, 834−843.

(21) Su, G.; Czader, A.; Homous, D.; Bernardes, G.; Mateen, S.; Cheung, M. S. Multiscale Simulation on a Light-harvesting Molecular Triad. *J. Phys. Chem. B* **2012**, *116*, 8460−8473.

(22) Balamurugan, D.; Aquino, A. J.; de Dios, F.; Flores, L., Jr.; Lischka, H.; Cheung, M. S. Multiscale Simulation of the Ground and Photo-Induced Charge-Separated States of a Molecular Triad in Polar Organic Solvent: Exploring the Conformations, Fluctuations, and Free Energy Landscapes. *J. Phys. Chem. B* **2013**, *117*, 12065−12075.

(23) Olguin, M.; Basurto, L.; Zope, R. R.; Baruah, T. The effect of Structural changes on Charge Transfer States in a Light-harvesting Carotenoid-diaryl-Porphyrin-C60 Molecular triad. *J. Chem. Phys.* **2014**, *140*, 204309-1−204309-10.

DOI: 10.1021/acs.jpclett.5b00074
J. Phys. Chem. Lett. 2015, 6, 1231−1237

(24) Wu, Q.; Voorhis, T. V. Direct Optimization Method to study Constrained Systems with Density-Functional Theory. *Phys. Rev. A* **2005**, *72*, 024502−024505.
(25) Cances, E.; Mennucci, B.; Tomasi, J. A new Integral Equation Formalism for the Polarizable Continuum Model: Theoretical Background and Applications to Isotropic and Anisotropic Dielectrics. *J. Chem. Phys.* **1997**, *107*, 3032−3041.
(26) Mennucci, B.; Tomasi, J. Continuum Solvation Models: A new Approach to the Problem of Solute's Charge Distribution and Cavity Boundaries. *J. Chem. Phys.* **1997**, *106*, 5151−5158.
(27) Zheng, S.; Phillips, H.; Geva, E.; Dunietz, B. D. Ab-initio study of the Emissive Charge-Transfer states of Solvated Chromophore-Functionalized Silsesquioxanes. *J. Am. Chem. Soc.* **2012**, *134*, 6944−6947.
(28) Zheng, S.; Geva, E.; Dunietz, B. D. Solvated charge transfer states of functionalized anthracene and tetracyanoethylene dimers: A computational study based on a range separated hybrid functional and charge constrained self-consistent field with switching Gaussian polarized continuum models. *J. Chem. Theor. Comput.* **2013**, *9*, 1125−1131.
(29) Phillips, H.; Zheng, Z.; Geva, E.; Dunietz, B. D. Orbital Gap Predictions for Rational Design of Organic Photovoltaic Materials. *Opt. Electron.* **2014**, *15*, 1509−1520.
(30) Lee, M. H.; Dunietz, B. D.; Geva, E. Calculation from First Principles Intramolecular Golden-rule rate constants for Photoinduced Electron Transfer in Molecular Donor-Acceptor Systems. *J. Phys. Chem. C* **2013**, *117*, 23391−23401.
(31) Lee, M. H.; Geva, E.; Dunietz, B. D. Calculation from First-Principles of Golden Rule Rate Constants for Photoinduced Subphthalocyanine/Fullerene Interfacial Charge Transfer and Recombination in Organic Photovoltaic Cells. *J. Phys. Chem. C* **2014**, *118*, 9780−9789.
(32) Manna, A. K.; Dunietz, B. D. Communication: Charge-transfer Rate Constants in Zinc-Porphyrin-Porphyrin-derived dyads: A Fermi Golden Rule First-Principles-Based Study. *J. Chem. Phys.* **2014**, *141*, 121102-1−121102-4.
(33) Lee, M. H.; Dunietz, B. D.; Geva, E. Donor-to-Donor vs Donor-to-Acceptor Interfacial Charge Transfer States in the Phthalocyanine-Fullerene Organic Photovoltaic System. *J. Phys. Chem. Lett.* **2014**, *5*, 3810−3816.
(34) Rizzi, A. C.; van Gastel, M.; Liddell, P. A.; Palacios, R. E.; Moore, G. F.; Kodis, G.; Moore, A. L.; Moore, T. A.; Gust, D.; Braslavsky, S. E. Entropic Changes Control the Charge Separation Process in Triads Mimicking Photosynthetic charge separation. *J. Phys. Chem. A* **2008**, *112*, 4215−4223.
(35) Marcus, R. A. On the Theory of Oxidation-Reduction Reactions Involving Electron Transfer. I. *J. Chem. Phys.* **1956**, *24*, 966−978.
(36) Marcus, R. A. Electrostatic Free Energy and Other Properties of States Having Nonequilibrium Polarization. I. *J. Chem. Phys.* **1956**, *24*, 979−989.
(37) Marcus, R. A. Electron transfer reactions in chemistry. Theory and experiment. *Rev. Mod. Phys.* **1993**, *65*, 599−610.
(38) Baer, R.; Neuhauser, D. Density Functional Theory with Correct Long-Range Asymptotic Behavior. *Phys. Rev. Lett.* **2005**, *94*, 043002.
(39) Livshits, E.; Baer, R. A well-tempered density functional theory of electrons in molecules. *Phys. Chem. Chem. Phys.* **2007**, *9*, 2932−2941.
(40) Stein, T.; Eisenberg, H.; Kronik, L.; Baer, R. Fundamental Gaps in Finite Systems from Eigenvalues of a Generalized Kohn-Sham Method. *Phys. Rev. Lett.* **2010**, *105*, 266802.
(41) Wilcox, D. E.; Lee, M. H.; Sykes, M. E.; Niedringhaus, A.; Geva, E.; Dunietz, B. D.; Shtein, M.; Ogilvie, J. P. Ultrafast Charge-Transfer Dynamics at the Boron Subphthalocyanine Chloride/C60 Heterojunction: Comparison between Experiment and Theory. *J. Phys. Chem. Lett.* **2015**, *6*, 569−575.
(42) Vosko, S.; Wilk, L.; Nusair, M. Accurate Spin-Dependent Electron Liquid Correlation Energies for Local Spin Density Calculations: a Critical Analysis. *Canadian J. Phys.* **1980**, *58*, 1200−1211.
(43) Lee, C.; Yang, W.; Parr, R. G. Development of the Colle-Salvetti Correlation-energy Formula into a Functional of the Electron Density. *Phys. Rev. B* **1988**, *37*, 785−789.
(44) Becke, A. D. Density-functional thermochemistry. III. The role of exact exchange. *J. Chem. Phys.* **1993**, *98*, 5648−5652.
(45) Stephens, P.; Devlin, F.; Chabalowski, C.; Frisch, M. Ab Initio Calculation of Vibrational Absorption and Circular Dichroism Spectra Using Density Functional Force Fields. *J. Phys. Chem.* **1994**, *98*, 11623−11627.
(46) Kuritz, N.; Stein, T.; Baer, R.; Kronik, L. Charge-Transfer-Like $\pi \rightarrow \pi^*$ Excitations in Time-Dependent Density Functional Theory: A Conundrum and Its Solution. *J. Chem. Theor. Comput.* **2011**, *7*, 2408−2415.
(47) Voityuk, A. A.; Rosch, N. Fragment Charge Difference Method for Estimating Donor-Acceptor Electronic Coupling: Application to DNA π-stacks. *J. Chem. Phys.* **2002**, *117*, 5607−5616.
(48) Lange, A. W.; Herbert, J. M. Polarizable Continuum Reaction-Field Solvation Models Affording Smooth Potential Energy Surfaces. *J. Phys. Chem. Lett.* **2010**, *1*, 556−561.
(49) Lange, A. W.; Herbert, J. M. A Smooth, Nonsingular, and Faithful Discretization scheme for Polarizable Continuum Models: The Switching/Gaussian Approach. *J. Chem. Phys.* **2010**, *133*, 244111-1−244111-15.
(50) Lange, A. W.; Herbert, J. M. Symmetric versus Asymmetric Discretization of the Integral Equations in Polarizable Continuum Solvation models. *Chem. Phys. Lett.* **2011**, *509*, 77−78.
(51) Muegge, I.; Qi, P. X.; Wand, A. J.; Chu, Z. T.; Warshel, A. The Reorganization Energy of Cytochrome c Revisited. *J. Phys. Chem. B* **1997**, *101*, 825−836.
(52) King, G.; Warshel, A. Investigation of the Free Energy Functions for Electron Transfer reactions. *J. Chem. Phys.* **1990**, *93*, 8682−8692.
(53) Schulten, K.; Tesch, M. Coupling of Protein Motion to Electron Transfer: Molecular Dynamics and Stochastic Quantum Mechanics Study of Photosynthetic Reaction Centers. *Chem. Phys.* **1991**, *158*, 421−446.

DOI: 10.1021/acs.jpclett.5b00074
J. Phys. Chem. Lett. 2015, 6, 1231−1237